European Journal of Wood and Wood Products
https://doi.org/10.1007/s00107-022-01806-6

ORIGINAL ARTICLE

Analysis of poplar timber finger joints by means of Digital Image Correlation (DIC) and finite element simulation subjected to tension loading

Cristian Timbolmas[2] · Francisco J. Rescalvo[1] · María Portela[3] · Rafael Bravo[2]

Received: 14 June 2021 / Accepted: 24 February 2022

Abstract
Due to the strong demand for wood, and the need to reduce the carbon footprint in construction, fast-growing low-graded planted species like poplar are promising wood for the supply chain in the context of engineered wood products, EWPs. Finger joints constitute a key technology for the manufacture of long structural elements of EWPs. Thus, evaluation of the mechanical properties of finger joints is important when designing these structural members. This paper shows the results of mechanical behaviour in tension of poplar timber of the I-214 cultivar, for specimens with and without finger joints, using experiments monitored by DIC (Digital Image Correlation) and simulated by the Finite Element Method. For moderate and intermediate loads, the samples with finger joints showed behaviour similar to those without joints. However, the presence of the fingers decreased the mechanical properties of the modulus of elasticity in the longitudinal direction anywhere from 7.7 to 23.7%; and there was a decrease of around 27.5% in tensile strength. An agreeable correlation between the DIC results and FEM simulations is obtained for the longitudinal, transversal, and shear strain fields, thus demonstrating the high potential of both methodologies.

1 Introduction

Wood is a natural organic, anisotropic, and renewable material with excellent ecological properties, acting as a carbon sink and characterized by a low embodied energy. Timber is one of the most important materials used over centuries within the construction sector (Harte 2016). Nowadays, because the timber market is continually increasing, the need for elements with special shapes and higher spans has become overwhelming. Complex connection—mechanically or adhesively bonded— is a common demand. Finger joints are currently used to produce engineered wood products like glued laminated timber beams (glulam) for different construction sectors, including buildings, bridges, or sport halls. A main benefit/advantage of implementing finger joints is the possibility to avoid certain types of flaws (e.g., grain deviation, knots, cracks, etc.) and geometrical imperfections.

Splicing two timber pieces together has been a challenging and difficult task since the early stage of finger joint applications, and the manufacturing process is highly industrialized nowadays. Finger joint parameters are, therefore, observed to determine which are more closely related to the strength of a given specimen. Many compressive research works (Özçifçi and Yapıcı 2008; Hernández et al. 2011; Rao et al. 2012; Yeh and Lin 2012; Morin-Bernard et al. 2021) have been carried out, employing different finger joint lengths and pitch lengths, resulting in finger joints with different slopes. Experimental results have shown that the length of the finger is one key parameter affecting finger joint strength (Ayarkwa et al. 2000): fingers with relatively flat slopes and sharp tips could achieve a high strength finger joint, even for finger lengths shorter than the usual length in current practice. The applied end pressure is likewise a key parameter for the evaluation of a specimen's ultimate tensile strength, according to Bustos et al. (2011); under lower end pressure, numerous air bubbles could trigger a significant reduction in the tensile strength. It is also important to remark that higher pressure affords the greatest strength

✉ Francisco J. Rescalvo
rescalvo@ugr.es

[1] Building Engineering School, University of Granada, Campus de Fuentenueva s/n. 18071, Granada, Spain

[2] Department of Structural Mechanics, University of Granada, Campus de Fuentenueva s/n. 18071, Granada, Spain

[3] PEMADE. University of Santiago de Compostela. Campus de Lugo, Lugo, Spain

Published online: 13 March 2022

of the finger. However, Ayarkwa et al. (2000) noted that after a certain value (12 MPa) for the applied end pressure, the tensile strength of the finger joint does not significantly increase. There is moreover a risk of failure of the specimen by splitting.

In addition to these parameters, the stiffness and thickness of the adhesive would be highly relevant for finger strength. As Groom and Leichti (1994) stated, a stiff adhesive is recommended to reduce longitudinal and radial stress concentration at the finger base, while significantly reducing shear stress within the adhesive layer. Other important aspects regarding the behaviour of finger joints bonded with different adhesives and temperature-dependent behaviour were underlined by Frangi et al. (2012).

Numerical finite element simulations (Serrano and Gustafsson 1999) were developed based on nonlinear fracture mechanics to predict the behaviour of finger joints and to assess the influence of the finger joint strength when defects are located in the bond-line. Various authors (Oudjene and Khelifa 2009; Khennane et al. 2014; Tran et al. 2014; Khelifa et al. 2016) carried out further finite element models for timber members dealing with failure prediction, fracture modes, different damage definition criteria, tensile strength, and geometrical optimization of the finger joint.

The Digital Image Correlation technique (DIC) holds great possibilities for exploring full-field displacements and strain measurements in the realm of experimental mechanics. As a non-contact, optical method, DIC has proven to be an ideal tool for the study of material behaviour for a large range of products (Lava et al. 2009). DIC is traditionally used to analyse steel, concrete and thermoplastic behaviour, but not wood material (Quanjin et al. 2020).

In recent years, however, considerable and comprehensive numerical and experimental approaches have been used to address timber fracture characterization by means of DIC and the finite element method (FEM) (Dubois et al. 2012; Milch et al. 2017; Ostapska and Malo 2021a, b). As is well known, the joints are the most critical part of most of the timber structures, being designed as mechanical or adhesively bonded joints. For that reason, joint behaviour is an interesting research area for the application of DIC (Angelidi et al. 2018). Specific applications in determining the Poisson ratio of a ductile adhesive in tension and compression have been undertaken through DIC (Angelidi et al. 2017).

The present study is focused on experimental and numerical investigations of the I-214 poplar cultivar behaviour in tension, with and without finger joints. The study is centered on the linear elastic part of the analysis, since the modulus of elasticity is the main variable of interest for characterization of the specimens. However, to take into account the influence of the contact and cohesion at the finger joints, nonlinear contact and cohesive models that behave almost linearly until failure were used. The experimental campaign involved the optical evaluation of the specimen during testing by means of DIC. The main contribution of the paper is to characterize the mechanical behaviour of the poplar timber with and without finger joints through an experimental analysis supported by DIC monitoring and FEM simulation.

2 Materials and methods

2.1 Poplar wood and adhesive

The wood used for this work was extracted from a 9-year-old- poplar plantation of the cultivar I-214 (*Populus x Euroamericana* [Dode] Guinier) located nearby the city of Granada, Spain. From the logs, planks of 2000 mm length and a section of 35×75 mm were sawn and dried for 6 months in natural conditions, always ensuring proper ventilation and avoiding direct exposure to the sun or rain. The final moisture content (MC) of wood was $10 \pm 2\%$. To manufacture the finger joint samples, a monocomponent polyurethane adhesive was used. The density of the adhesive was 1.12 g/cm^3 and its viscosity (Brookfield RVT) was 7000 mPa.s, spindle-6, with a rotational speed of 20 rpm and with a temperature of 20 °C, measured between 16 and 36 h after production (ISO 2555:2018).

2.2 Sample description and manufacturing

A set of 20 poplar specimens were prepared to be subjected to tension in the grain direction. The samples were divided into two batches of 10 specimens each, without finger joints (TT) and with finger joints (TF), respectively, without being grouped into strength classes. All the specimens were sawn to a length of 586 mm, with a general cross-section of 50×17 mm. So as to promote failure in the central area of the specimen and to avoid undesired breakage, the width of this central part was narrowed to 20 mm, resulting in a mid-section of the specimen of 20×17 mm (Fig. 1). For the TF samples, the finger joint was located at the geometrical centre. The adhesive for the finger joint was applied at a temperature of 20 ± 2 °C, with a wood MC of $9.8 \pm 1.5\%$, complying with the requirements of the manufacturer for its application. The adhesive was applied at a rate of 250 g/m^2. After that, the specimens were prepared and introduced in a climatic chamber at 20 °C and 65% relative humidity, according to the EN 408:2010 + A1:2012 (2012) standard.

As Jokerst (1981) stated, the geometry of the finger joint dictates the strength of a joint, and consequently the strength of the specimen. Among the research findings reported to date, the finger length is found to mostly affect the strength of the finger joint, while the pitch has a negligible effect on joint strength. In addition, tip thickness and slope of the finger bear a noticeable impact on joint strength (Strickler

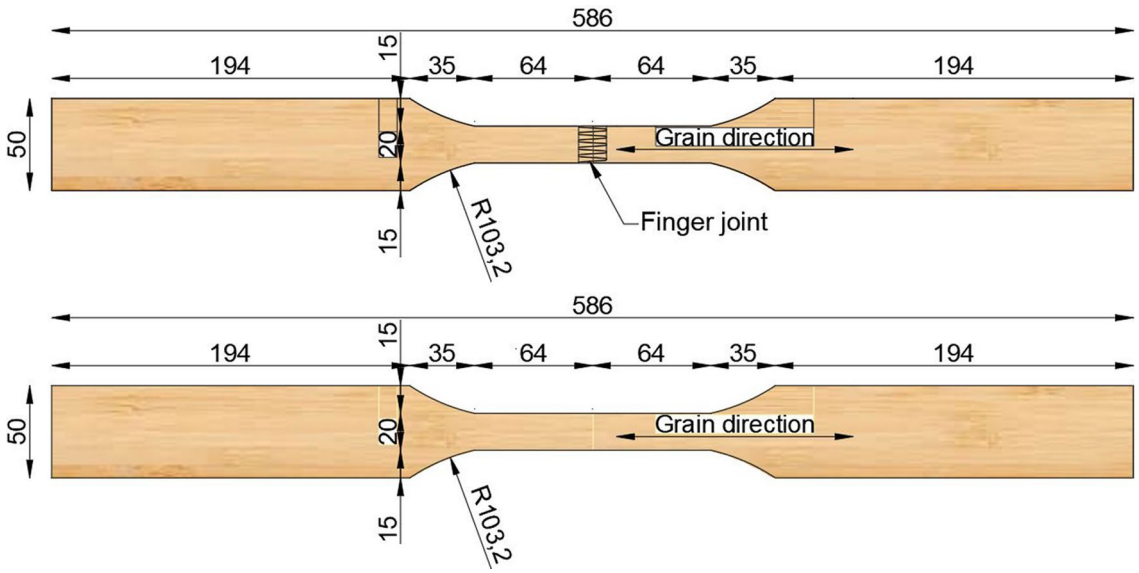

Fig. 1 Geometry of the tensile poplar specimens with (TF) and without (TT) finger joints. Dimensions in mm

1980). According to EN 14080:2013 (2013)—Annex I, the geometric parameters that define a joint include the finger length (l_j), finger pitch (p), finger angle (α), tip gap (l_t), and tip width (b_t) (see Fig. 2). These parameters are interrelated, meaning that a change in one parameter will influence all the others. This complicates research of the effect of any single parameter on strength (Jokerst 1981). According to studies on the performance of finger joints (Hu et al. 2012; Habipi and Ajdinaj 2015), good performance in terms of tensile strength and modulus of elasticity can be attained for finger lengths of 13–14 mm; hence, a length of 14 mm was selected for the specimens used here (Fig. 2). Afterwards, the geometric parameters of the finger joint were set to fulfil the requirements stated in Annex I from EN 14080:2013 (2013) (see Fig. 2). Taking into account the length of the finger joint, a final pressure of 10 N/mm^2 was applied, in view of the graph from Annex I (EN 14,080:2013).

2.3 Experimental test

Tensile tests were carried out in a multi-testing machine, specially manufactured (ad hoc) by Microtest S.A Company, with an electrical actuator having a maximum capacity of 200 kN, with an accuracy of 0.01 kN, and a speed test rate of 0.5 mm/s. To avoid slipping during the test, the samples were clamped 90 mm on each side. Figure 3 shows the setup of the experiment with the DIC equipment during a test. The

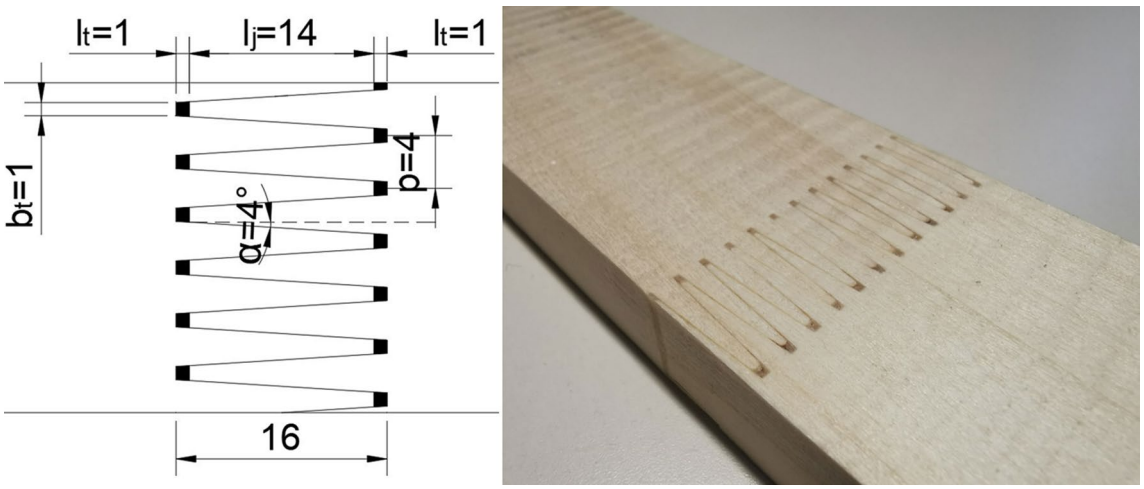

Fig. 2 Geometrical parameters of the finger joint profile and finger joint picture. Dimensions in mm

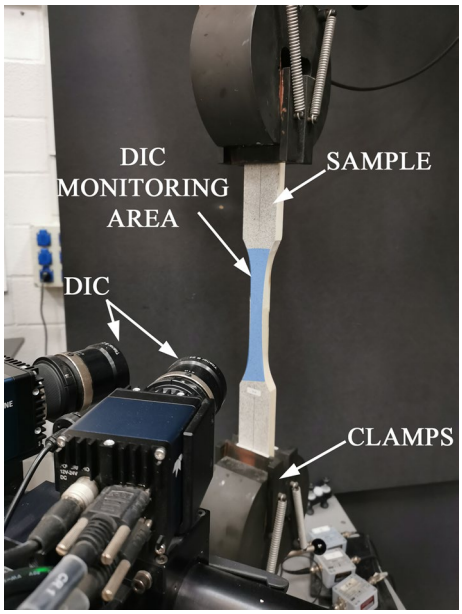

Fig. 3 Axial tensile test set-up with DIC equipment

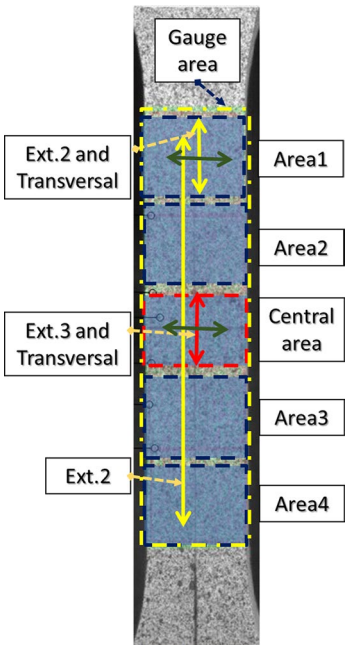

Fig. 4 Definition of the virtual extensometer position: Ext.1, Ext.2, Ext. 3, Gauge area in dot and dash line and areas for strain determination dash line

maximum tensile strength ($f_{t,0}$) was computed according to EN408:2010 + A1:2012 (2012) standard as:

$$f_{t,0} = \frac{F_{max}}{A} \tag{1}$$

where F_{max} is maximum axial load, and A is the cross-section of the specimen at the mid-length.

2.4 Digital image correlation

For monitoring the strain field in the central part of the specimens, a three-dimensional image correlation non-contact optical measurement system was used, Aramis 3D® (GOM mbH, Braunschweig, Germany). The ARAMIS 3D System is a powerful non-contact measuring instrument that is suitable for assessing three-dimensional deformation and strain distributions of real components under static or dynamic loads.

The surface of the specimen should be smooth and clean. Then, a black-on-white random speckle pattern was applied as uniformly as possible, using an opaque spray paint on the face of each sample.

The DIC system was calibrated using the specific Aramis 3D calibration protocol, which includes camera positions and lens distortion parameters. With this calibration information, the system ensures measurement accuracy. The DIC monitoring area is defined by a face size with 19 pixels, as well as 16 pixels for point distance.

The optical module of Aramis (made up of two 12 M industrial cameras) was oriented towards the specimen surface. The placement of the Aramis optical module was also conditioned by the recommended calibration distance to the specimen, in this case 295 mm, with an angle of 25º between cameras.

By means of this technique and the capabilities of GOM Correlate software, developed by GOM GmbH (2020), the modulus of elasticity in tension was calculated using two methods: (I) Based on the relationship established in the standard EN 408:2010 + A1:2012 (2012); (II) based on the average stress–strain relation, within the defined area.

For method I, according to standard EN 408:2010 + A1:2012 (2012), the following relation was used:

$$E_{t,0} = \frac{l_1(F_2 - F_1)}{A(w_2 - w_1)} \tag{2}$$

where $F_2 - F_1$ are the increment of load on the straight line portion of the load deformation curve at 20–30% of the maximum load, $w_2 - w_1$ are the increment of the corresponding displacement, l_1 is the length of the extensometer and A is the cross-section of the specimen at the mid-length. To derive accurate and reliable results, three pairs of virtual orthogonal extensometers with different lengths were placed in three distinct locations (Fig. 4-left). The first extensometer, Ext.1, was placed along the evaluation area (100 mm length) in accordance with EN 408:2010 + A1:2012 (2012) for $E_{t,0}^{Ext.100}$ computation. The second extensometer, Ext.2, was placed at the top end of the gauge length at a length of

20 mm ($E_{t,0}^{Ext.20}$) for control of the results. To evaluate the influence of the finger, a third extensometer (Ext. 3) was placed within the middle of the finger joint at a length of 14 mm to calculate $E_{t,0}^{Ext.14}$. In all cases, to calculate Poisson's ratio, horizontal virtual extensometers 15 mm in length (Transversal and Transversal 1) were placed at the mid-length of the vertical ones. Thus, the relationship between transversal and longitudinal strains could be computed.

In the case of method II, since the DIC technique allows one to determine the mean strains of a defined area with different geometric sizes (Fig. 4-center and right), several areas were considered, starting from the mid-gauge length to the ends of the specimens. To determine the mean longitudinal strain corresponding to these areas, for the specimen with no finger joint, a gauge area corresponding to the entire gauge length was defined, allowing for computation of the corresponding modulus of elasticity ($E_{t,0}^{ga}$) (see Fig. 4-center).

For the specimens with finger joints, the modulus of elasticity is calculated in several distinct areas: $E_{t,0}^{c.a}$ corresponding to the central area, $E_{t,0}^{a1}$ to "Area 1", and so on (see Fig. 4-right). These moduli are computed as the slope of corresponding stress–strain relation between the interval of 20%-30% of the maximum load (EN 408:2010 + A1:2012).

For both methods, Poisson's ratio of the specimen was computed. To this end, two different values of Poisson's ratio were obtained employing methods I (υ) using the extensometer, Ext. 3, and II (υ^*) using the defined central area, respectively, as follows,

$$\upsilon = -\frac{\Delta\varepsilon_{transv}}{\Delta\varepsilon_{axial}} \tag{3}$$

where $\Delta\varepsilon_{transv}$ is the transversal strain increment (method I) or the transversal average strain (method II), and $\Delta\varepsilon_{axial}$ is the longitudinal strain increment (method I) or the longitudinal average strain (method II).

2.5 Finite element method: numerical simulations

A 3D parametric finite element model to investigate the behaviour in tension of the specimens with and without finger joints was developed employing Abaqus software (Abaqus CAE 2020) and the programming language Python (Python Core Team 2015). Figure 5 depicts the finite element model of the sample with finger joints. This 3D solid linear material elastic anisotropic model is composed of two glued parts that interact along the finger interface by contact. The mechanical behaviour of the interface is governed by contact and damage cohesive traction laws from Abaqus (Camanho et al. 2003; Abaqus CAE 2020). The failure criterion used for this study is the quadratic traction law.

The boundary conditions are defined according to the experimental test set-up; hence, they were modelled as

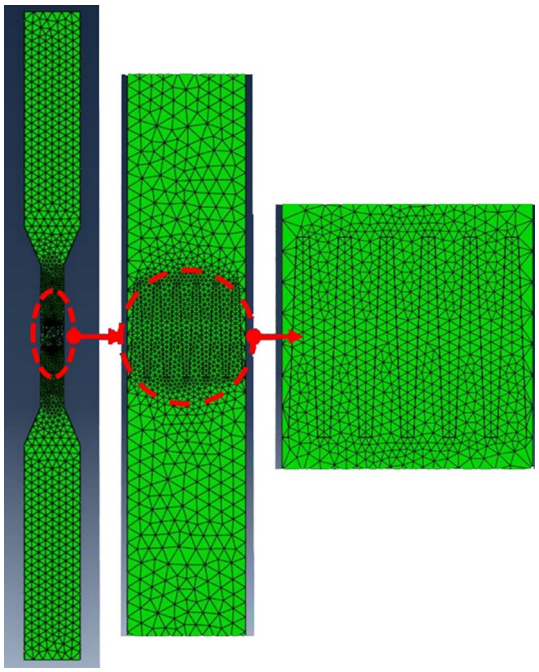

Fig. 5 FEM mesh: general view of the specimen (left), mesh detail of the fingers joint (middle and right)

clamped conditions applied to the all-lateral area of the bottom flange of the specimen. For the top flange, however, the boundary conditions allowed the imposed longitudinal displacement of the specimen with a constant rate of 0.4 mm/s, similar to the experimental part. In the case of the TF samples, the failure of the model is brittle due to the opening of the contacts between fingers. Owing to the sharp geometry of the fingers, a four-node tetrahedral element (C3D4) was used for the modelling of the specimen. The meshing process was refined in the surrounding finger area, with a mean element size of 0.8 mm for the fingers. For the rest of the gauge length, the mean size was 2.4 mm, and the coarse size corresponds to the tapered part and clamping area with mean sizes of 6.4 mm and 7.4 mm, respectively. The size geometry of the meshing process was changed based on converge analysis until the results were stable.

The constitutive parameters as moduli of elasticity, Poisson's ratio, and the contact parameters are defined in Tables 1 and 2. The longitudinal input elastic parameter (E_1) was taken from the performed experiments, while the rest of the elastic input parameters were considered as a ratio of 1/8 for E_2/E_1, and 1/30 for E_3/E_1, taken close to the ratios corresponding to "Yellow Poplar" wood (Table 5–1 from Wood Handbook 2010). In turn, the input parameters for the contact interface were defined in view of previous, similar numerical simulations (Tran et al. 2014). An iterative calibration process modifying the initial parameters from the reference was performed by trial and successive

Table 1 Input elastic parameters for FEM simulations

Specimen	E_1 (MPa)	E_2 (MPa)	E_3 (MPa)	G_{12} (MPa)	G_{13} (MPa)	G_{23} (MPa)	$\upsilon_{12}=\upsilon_{13}=\upsilon_{23}$
TT	9936	1244	331	759	557	278	0.40
TF	8356	1044	278	759	557	278	0.40

E_1, E_2, E_3 are the moduli of elasticity in longitudinal, transversal and radial directions; G_{12}, G_{13}, G_{23} are the shear moduli in longitudinal, transversal and radial planes; υ_{12}, υ_{13}, υ_{23}, are the Poisson ratio

Table 2 Input contact parameters for FEM simulations

Specimen	Friction coefficient	Normal penalty stiffness (N/mm)	Tangential penalty stiffness (N/mm)	K_{nn} (N/mm^2/mm)	$K_{tt}=K_{ss}$ (N/mm^2/mm)	σ_n (N/mm^2)	$\tau_{nI}=\tau_{nII}$ (N/mm^2)	δ_p (mm)
TF	0.3	1E+09	1E+09	5.5	62	4.6	8.5	0.001

K_{nn}, K_{tt}, K_{ss} are the normal, tangential and radial stiffness; σ_n, τ_{nI}, τ_{nII} are the maximum nominal interfacial strength in the normal and shear direction I and II; δ_p is the effective plastic displacement

verification until the numerical model had fitted the experimental relation.

3 Results and discussion

3.1 Experimental results

All the manufactured specimens, TT and TF, were subjected to the static axial tensile test. Figure 6 shows the stress–strain relations based on method I using extensometer with 100 mm length (top), based on method II, using mean longitudinal strains from the central area (Fig. 6 bottom-left), and method I, using the extensometer of 14 mm length (Fig. 6 bottom-right).

All the relations highlighted linear-elastic behaviour without any evidence of plastic deformation until failure of the specimens, so that the failure is characterized by brittle failure. Clearly the TF specimens exhibit lower stiffness than the TT specimens, identified by a slight curvature within the stress–strain relation induced by the non-linear behaviour of the finger joint.

For the TF specimens with an extensometer or area located at the finger joint, the relations are slightly lower due to the strain concentration captured by DIC at the base of the fingers. Therefore, this local effect produces a slight reduction in the moduli of elasticity.

Tables 3 and 4 show the longitudinal moduli of elasticity using methods I and II, for the extensometer of 100 mm length ($E_{t,0}^{Ext.100}$) according to EN 408:2010 + A1:2012, the corresponding area ($E_{t,0}^{ga}$) of the extensometer located in the finger joint or mid-gauge length for the specimen without finger ($E_{t,0}^{Ext.14}$) and its corresponding central area ($E_{t,0}^{ca}$). The third extensometer is located away from the finger joint at 20 mm length ($E_{t,0}^{Ext.20}$) and a corresponding area that coincides with the extensometer location ($E_{t,0}^{a2}$). It is important to remark that in Table 4, the results computed based on the gauge area with method II are not meaningful, given the reduced size of the finger area (about 14 mm length) compared to the entire gauge area (area of finger joints is 11% of the gauge area). Thus, the mean longitudinal strain using the gauge area is representative only for the TT specimens, since the strain is homogeneous, giving values that match the results provided by method I using Ext.1 ($E_{t,0}^{Ext.100}$). For the TT specimens, the moduli of elasticity are considerably higher than for the TF specimens, considering that the finger joint introduces a weakness in the longitudinal behaviour of the specimen.

For the TT specimens, Table 3 shows that the mean values obtained by means of method I and method II are comparable, ranging between 8495 N/mm^2 and 9120 N/mm^2. For the specimens with finger joints (TF), Table 4 shows that the mean values employing methods I and II have a wider range, 6942 N/mm^2–7736 N/mm^2, possibly induced by different strength classes of the top and bottom timber pieces. These higher differences related to the finger specimens are directly linked with the strain acquisition using method II, which is able to capture the high strain concentration. Consequently, the mean longitudinal strains are high, resulting in low longitudinal moduli values. Under method I, the displacements are computed by integration of the strains, for which reason the influence of the concentration of strains is averaged.

The last row in Table 4 shows the moduli reduction between TT and TF, which varies from 11.0 to 19.0%, indicating a relatively low dispersion of the results that is mainly induced by the finger joint and the lack of timber part classification in strength classes. The maximum reduction (19.0%) is found for the measurements located in the central area (finger joint) using method II. In this local measurement, high strains are captured by DIC, increasing the mean longitudinal strain. Hence, the computation of the modulus of elasticity in this area provides reduced values. For the same

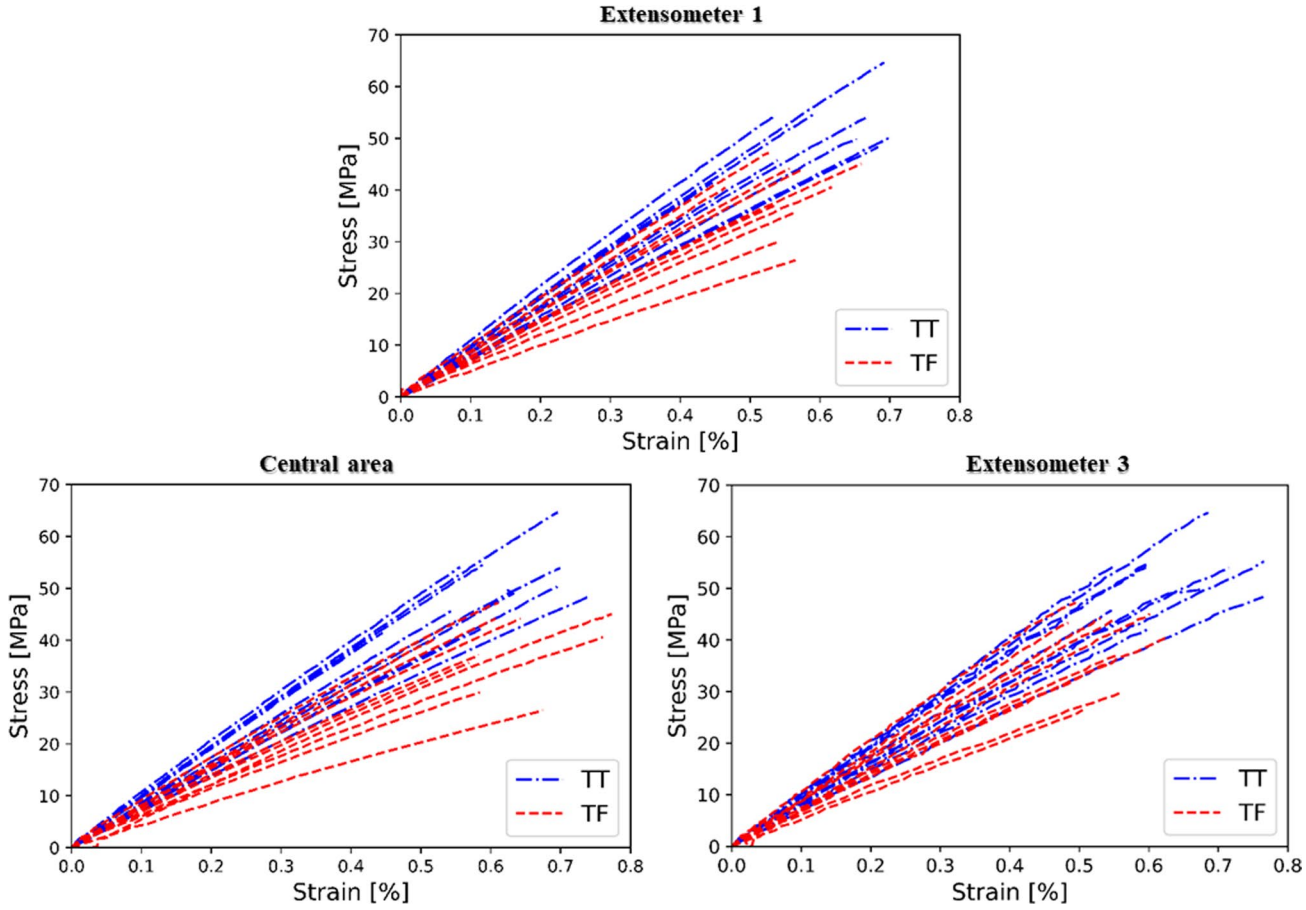

Fig. 6 Stress–strain relations for TT and TF specimens: (top) based on Ext. 1; (bottom-left) based on defined central area; (bottom-right) based on Ext. 3

Table 3 Results for the TT specimens and the corresponding mean value

Specimen name	$E_{t,0}^{Ext.100}$ (N/mm^2)	$E_{t,0}^{ga}$ (N/mm^2)	$E_{t,0}^{Ext.14}$(N/mm^2)	$E_{t,0}^{ca}$ (N/mm^2)	$E_{t,0}^{Ext.20}$ (N/mm^2)	$E_{t,0}^{a2}$ (N/mm^2)
TT1	7916	9755	7529	9710	7606	9942
TT2	7611	7562	7793	7827	7247	7218
TT3	7533	7421	7926	7481	7590	7602
TT4	7531	7468	7740	7494	7396	7853
TT5	8627	8545	8124	8294	8275	8368
TT6	8661	8695	8990	8741	8844	9557
TT7	10,652	10,553	12,128	10,689	10,852	11,022
TT8	6527	9342	8920	9296	9610	10,396
TT9	6402	9341	9225	9302	9784	10,424
TT10	7487	7398	6789	7040	8675	8822
Mean (MPa)	8495	8608	8516	8587	8588	9120

location, the reduction is very similar to the one provided by method I, with a variation of 0.5%. This trend is visible for all of the cases since the virtual extensometers do not take into account the local nonlinear strain concentrations developed at the fingers. With regard to the obtained results using methods I and II for the top part of the specimen (Ext. 2 and Area 2), the maximum mean reduction is 16.4% and 11.0%, which highlighted the highest variation (5.4%) between methods. Consequently, the mean variation value of modulus of elasticity in tension, evaluated according to the

Table 4 Results for the TF specimens, the corresponding mean value, and the differences (ΔTF-TT %) between TT and TF specimens

Specimen name	$E_{t,0}^{Ext.100}$ (N/mm^2)	$E_{t,0}^{ga}$ (N/mm^2)	$E_{t,0}^{Ext.14}$(N/mm^2)	$E_{t,0}^{ca}$ (N/mm^2)	$E_{t,0}^{Ext.20}$ (N/mm^2)	$E_{t,0}^{a2}$ (N/mm^2)
TF1	8079	–	8449	7817	8082	8925
TF2	7884	–	7164	6952	9489	7455
TF3	9036	–	7882	8971	10,453	8191
TF4	7182	–	7008	7015	8093	6613
TF5	7297	–	7741	6835	7088	8193
TF6	9356	–	9215	8910	9470	10,840
TF7	5669	–	5302	5526	5194	7006
TF8	6468	–	5403	5982	7739	7028
TF9	4944	–	5486	4923	4246	4391
TF10	6647	–	5772	6611	6582	7612
Mean (MPa)	7256	–	6942	6954	7644	7625
$\Delta_{TT\text{-}TF}$ (%)	14.6	–	18.5	19.0	11.0	16.4

EN 408:2010 + A1:2012 (2012) standard, is around 14.6%, mainly due to the finger joint presence.

Table 5 summarizes the average value of the experimental results and the mean difference related to the Poisson ratios obtained using methods I-II (ν and ν*)—using the extensometer with 10 mm length (Ext. 3) and central area, tensile strength ($f_{t,0}$) and density (ρ) of the TT and TF specimens. As the current results revealed, the finger joints do not have any influence on Poisson's ratio value, because the fingers do not significantly affect the transversal strains. Yet a significant reduction (27.5%) in the tensile strength is observed for the TF specimens, because the weakness induced in the longitudinal direction triggered a failure mechanism. According to EN 14080:2013 (2013), the tensile strength obtained for the TF samples is higher than that required for the maximum resistance class, GL32h / GL32c.

Table 5 Mean Poisson ratio using method I (ν) with Ext. 3, and II (ν*) with central area, mean tensile strength parallel to the grain (ft,0), mean density and variation in (ΔTF-TT) %

Specimen name	ν	ν*	$f_{t,0}$ (N/mm^2)	ρ (kg/m^3)
TT	0.40	0.40	51.0	385
TF	0.40	0.42	37.0	375
$\Delta_{TF\text{-}TT}$ (%)	0.0	5.0	− 27.5	− 2.6

An important aspect deserving mention is that, for both specimens, the mean Poisson ratios computed using both approaches (Methods I and II) are nearly identical (0.0% and 5.0% of variation). Therefore, the proportionality between transversal and longitudinal deformation is similar for both computational methods. Subsequently, the presence of the finger joint does not exert any influence related to density (− 2.6%).

For a better understanding of the longitudinal moduli variation along the gauge length, the mean strains computed based on the defined areas (Fig. 4) –Method II, are

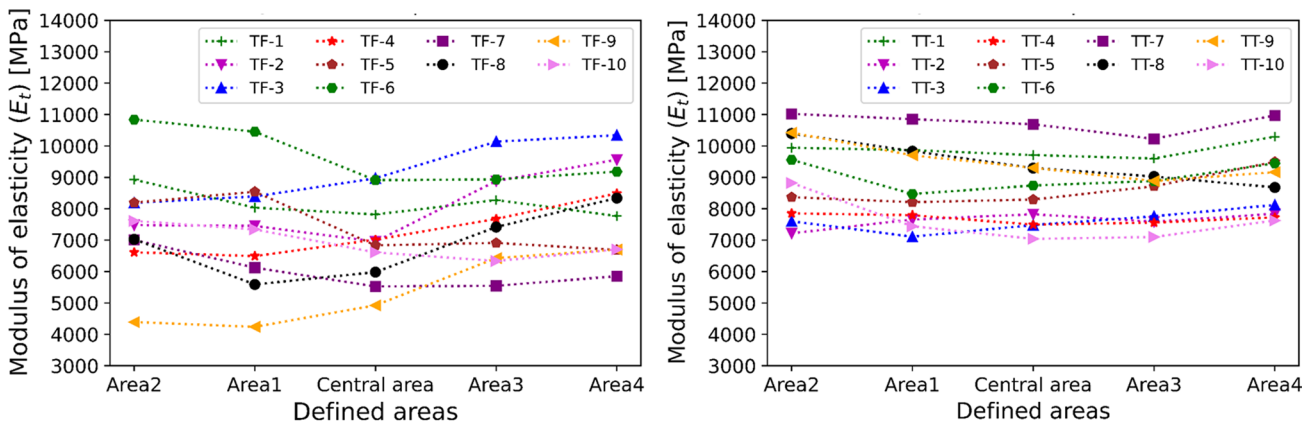

Fig. 7 Modulus of elasticity variation of the specimens with finger joints-TF (left) and without finger joints-TT (right)

Fig. 8 Failure pattern of the TT (**a**) and TF (**b**) specimens

used for the longitudinal moduli computation. The corresponding moduli distributions are shown in Fig. 7. It is worth mentioning that for the TF specimens, a significant decrease is emphasized in the central area, corresponding to the finger joint location. However, the TT specimens revealed a homogeneous distribution of longitudinal moduli along the gauge length, mainly due to the absence of the finger and therefore to the one-piece manufacturing process of the specimen. It is moreover important to remark that for the TF specimens, different moduli values are observed for the top and bottom part of the specimen, indicating different timber strength classes used in the manufacturing process.

In general, for the TT specimens, the failure is mainly caused by crack propagation along the matrix, while initiation of the failure is triggered within the tapered part (transition between gauge and top flange) (see Fig. 8a). Yet for the TF specimens, the failure is brittle and the crack initiation is located within the finger joint, developing in the direction perpendicular to the fingers (see Fig. 8b).

Figure 9 shows the normal distributions of the mean moduli of elasticity presented in Tables 3 and 4, based on the considered computation methods (I and II). As Fig. 9 shows, the mean longitudinal strain distributions for specimen TT, using method I (left), are similar and identical from the pattern variation point of view, while for TF specimens, a visible decrease and a higher dispersion are revealed by the distribution (Fig. 9left).

This heterogenic aspect of the results is likewise observed in the results based on method II (Fig. 9right).

Figure 10 shows the experimental longitudinal strain evolution for one representative TT (top) and TF (bottom) specimen with intermediate behaviour. In addition, the corresponding DIC strain map is shown at four loading stages: 25%, 50%, 75% and 100%, respectively.

As the DIC strain map shows, for low and intermediate load step levels (up to 50% of the maximum load), the strain field is homogeneous for both specimens. For the TF specimen, the force–elongation relation also captures the stiffness reduction, characterized by a reduced slope compared to the TT relation.

For higher load levels, several inhomogeneities start to appear for TF around the fingers due to the non-linear behaviour of the finger joint, while for TT the field is still homogeneous in the mid-section of the specimen. For loads closer to the fracture point, the strain field remains homogenous for TT, but for the TF specimen, a significant concentration

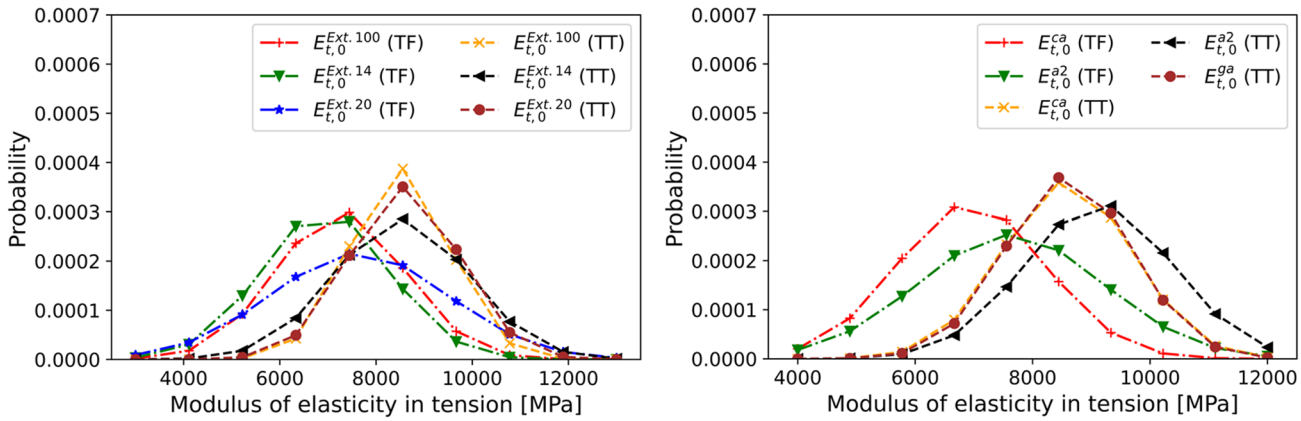

Fig. 9 Distribution of modulus of elasticity using: extensometers—method I (left); defined areas—method II (right)

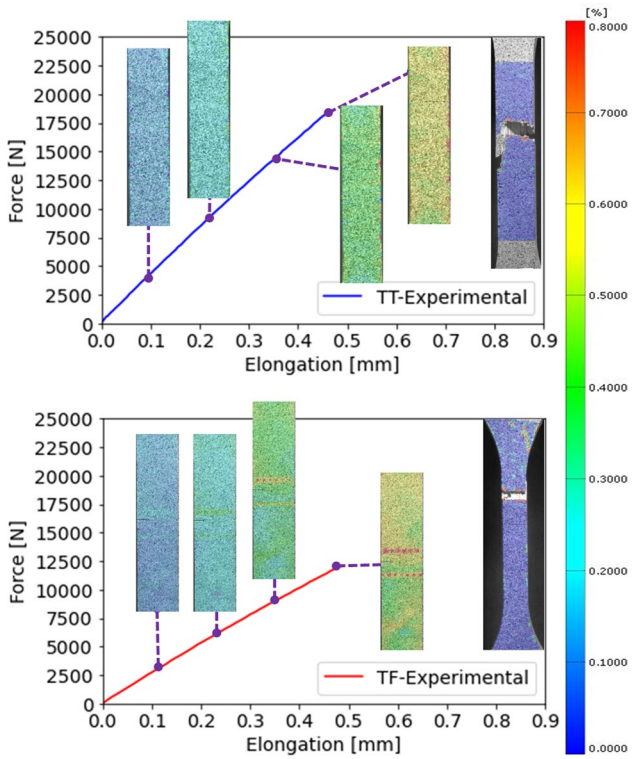

Fig. 10 Experimental force–elongation curve and DIC vertical strains field at four different load steps for one representative TT (top) and TF (bottom) specimen

of strains is reflected by the high nonlinearities in the finger interface.

3.2 Finite element simulation and DIC results

For the discussion of this subsection, a representative experimental sample and a calibrated numerical model were selected. Figure 11 presents the force–elongation relations for the TF and TT specimens obtained from the experimental and numerical simulation part. The relations from the experimental part are plotted in a representative sample with an intermediate behaviour based on the relations provided in Fig. 6-top. The numerical simulations through the calibration process matched the experimental relation and the failure point of the specimens. The calibration process started with the experimental parameters; then, through successive steps, the final values were obtained. These parameters of the FEM calibrated models are presented in Tables 2 and 3.

Figure 12 shows a comparison of the longitudinal (ε_x), transverse (ε_y) and shear (ε_{xy}) strain fields between DIC and FEM before failure. Both techniques capture the high strain concentration around the tip and base of the fingers due to the initiation of detachment of the fingers and the shear distortion along the lateral faces. The maximum longitudinal strain concentration occurs within the base of the fingers, giving similar values for DIC and FEM (0.8%). It is noteworthy that longitudinal strains within the tip are almost null due to the gap produced during the manufacturing process. The maximum longitudinal strain (ε_x) occurs at the base owing to the action of the cohesive forces along the lateral sides of the fingers, the strain flowing through the finger base. Regarding the transversal strains and shear strains, distributions by FEM and DIC are in accordance, showing low magnitude in comparison to the longitudinal one, with a maximum transversal strain of 0.3%, and 0.12% for shear strain. For the transversal (ε_y), the flow is symmetric and is mainly caused by the Poisson ratio, producing a small necking due to a high Poisson's ratio (value of 0.4 in Table 5). For the shear (ε_{xy}), the strains at the fingers are equal and opposite, and the maximum strains occur at the tips of fingers because of the reduced size of the section of the finger close to the tip. While the DIC shear strain distribution suggested small negative shear strains, which can be produced by the imperfections between the top and bottom clamps of the machine.

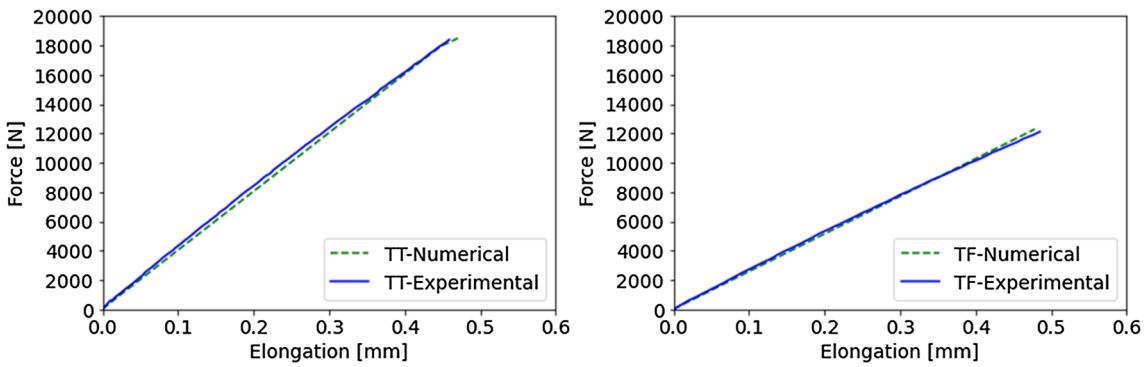

Fig. 11 Force–elongation of numerical and experimental relationships for TF specimen (left) and TT specimen (right)

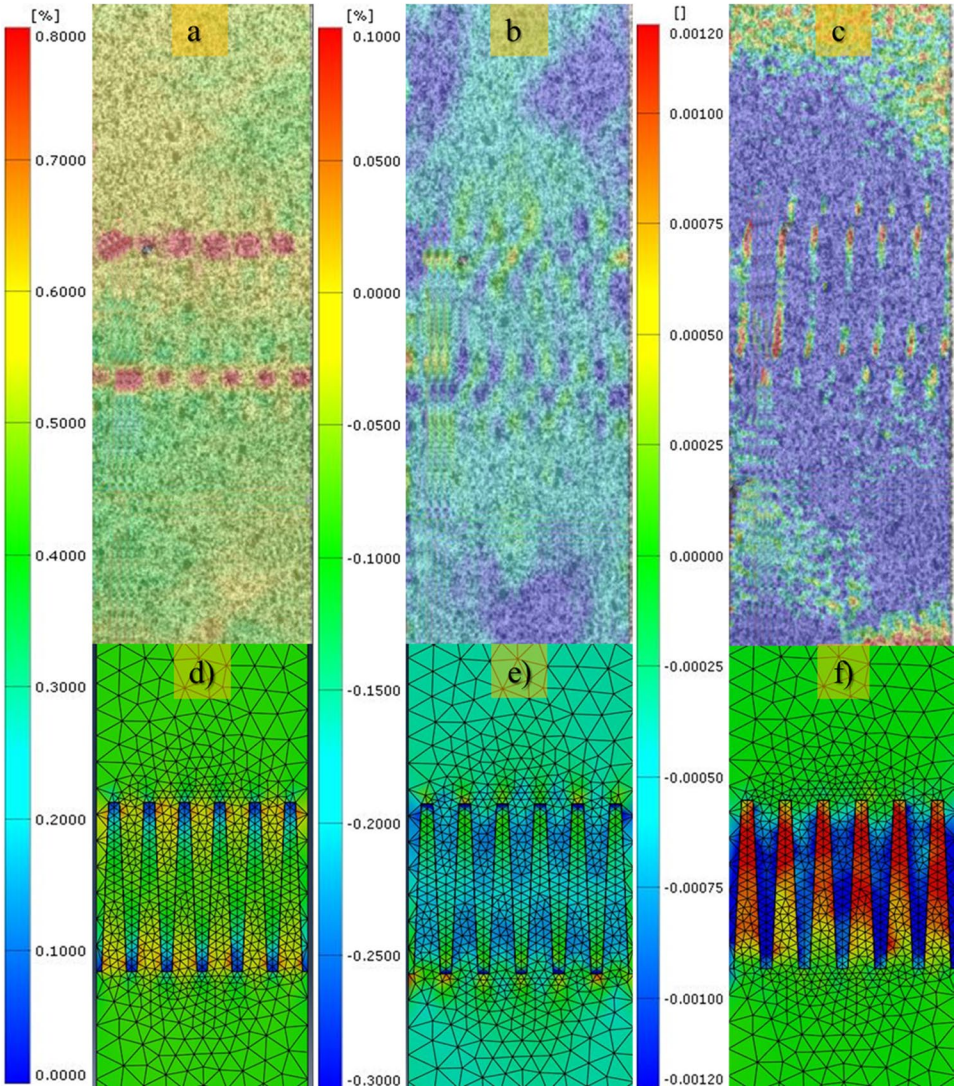

Fig. 12 Strain field distribution for TF specimen. **a** Longitudinal strain (ε_x); **b** Transversal strain (ε_y); **c** Shear strain (ε_{xy}) from DIC. **d** Longitudinal strain (ε_x); **e** Transversal strain (ε_y); **f** Shear strain (ε_{xy}) from FEM

4 Conclusion

This study analyzed and characterized the mechanical behaviour of the poplar timber of I-214 cultivar for specimens with and without finger joints. Based on the obtained results, the poplar wood behaviour subjected to axial tensile stress was analyzed in parallel with the numerical simulations.

The experimental results obtained employing different methodologies using DIC technique allow the possibility to analyze the samples along their entire length. As the results show, for the specimens with fingers joint, the reduction in the stiffness and the tensile strength becomes relatively small. The results show that the presence of the fingers decreases the mechanical properties between 11.0 and 19.0% for moduli of elasticity, and around 27.5% of the tensile strength, respectively. However, the tensile strength remains higher than the limits specified in EN 14080 standard.

One of the most important experimental results obtained by means of DIC technique is the evaluation of the longitudinal modulus of elasticity in tension along the gauge length of the specimen. Consequently, two particular behaviours are identified, a homogeneous moduli of elasticity distribution along the gauge length for the TT specimens, while for the TF specimens, the results were highly dispersed, with a minimum value located within finger joint. It is worth mentioning that both methods provide similar results for the strain gauges placed within finger length and the corresponding area of the finger surface. Nevertheless, the central area is averaging the strains of the entire length of the finger, which revealed high parts with high strains concentration. Therefore, the low variation of the mean reduction obtained employing both methods, confirms the validity of both investigation methods.

Besides, the DIC technique is a powerful tool that allows evaluating the strain state at every rate load, and the strain concentrations and flow within the finger geometry.

Furthermore, numerical simulations were carried out to obtain a suitable FE model, able to capture, verify and complement the structural behaviour provided by DIC, and showing good agreement. Through these numerical simulations, the main aim was to obtain the parameters related to the contact interface, which can be extended to a further study related to the optimization of fingers joints. The results provided through this study, are useful for further research tasks, which involve glued poplar beams or other engineered wood products, where the tension behaviour of the raw material has yet to be known.

Acknowledgements Acknowledgement is due to Dr. María A. Ripoll from the IFAPA for the supply of poplar wood, and the professor Antolino Gallego (University of Granada) for his support along the experimental campaing, data interpretation and review of the paper.

Author contributions CT: writing, analytical work and data analysis and interpretation; FR: writing, experimental work and experimental design; RB: supervision, writing, data analysis and interpretation; MP: supervision on experimental work and experimental design.

Funding Funding for open access charge: Universidad de Granada / CBUA. This work has been possible thanks to financial support of the COMPOP_Timber project "Desarrollo de productos de ingeniería elaborados a base de tablones y chapas de chopo con inserciones de material compuesto para su uso en construcción", BIA2017-82650-R and the SmartTimber project "Productos estructurales inteligentes de madera multiespecie para construcción industrializada baja en carbono", PID2020-114386RB-I00.

Data availability Not applicable.

Code availability The plots and scripts were built employing Python 3.8 software. The numerical simulations were performed using Abaqus CAE 2020 softaware (license provided by the Department of Structural Mechanics from University of Granada, Spain). The Digital Image Correlation (DIC) analysis was perfomerd using GOM Correlate 2020 software (license provided by PEMADE laboratory, Lugo, Spain).

Declarations

Conflict of interest The authors declare that they have no known competing financial interests or personal relationships that could have appeared to influence the work reported in this paper.

References

Abaqus CAE (2020) ABAQUS/Standard User's Manual, Version 2020

Angelidi M, Vassilopoulos AP, Keller T (2018) Ductile adhesively-bonded timber joints—Part 1: experimental investigation. Constr Build Mater 179:692–703. https://doi.org/10.1016/j.conbuildmat.2018.05.214

Angelidi M, Vassilopoulos AP, Keller T (2017) Displacement rate and structural effects on poisson ratio of a ductile structural adhesive in tension and compression. Int J Adhes Adhes 78:13–22. https://doi.org/10.1016/j.ijadhadh.2017.06.008

Ayarkwa J, Hirashima Y, Sasaki Y, Yamasaki M (2000) Influence of finger-joint geometry and end pressure on tensile properties of three finger-jointed Tropical African Hardwoods. South African for J 188:37–49. https://doi.org/10.1080/10295925.2000.9631268

Bustos C, Hernández RE, Beauregard R, Mohammad M (2011) Effects of end-pressure on the finger-joint quality of black spruce lumber: a microscopic analysis. Maderas Cienc y Tecnol 13:319–328. https://doi.org/10.4067/S0718-221X2011000300007

Camanho PP, Davila CG, de Moura MF (2003) Numerical simulation of mixed-mode progressive delamination in composite materials. J Compos Mater 37:1415–1438. https://doi.org/10.1177/0021998303034505

Dubois F, Méité M, Pop O, Absi J (2012) Characterization of timber fracture using the digital image correlation technique and finite element method. Eng Fract Mech 96:107–121. https://doi.org/10.1016/j.engfracmech.2012.07.008

EN 408:2010 + A1:2012 (2012) Timber structures. Structural timber and glued laminated timber. Determination of some physical and mechanical properties. European Committee for Standardization (CEN)

EN 14080:2013 (2013) Timber structures. Glued laminated timber and glued solid timber. Requirements. European Committee for Standardization CEN

Frangi A, Bertocchi M, Clauß S, Niemz P (2012) Mechanical behaviour of finger joints at elevated temperatures. Wood Sci Technol 46:793–812. https://doi.org/10.1007/s00226-011-0444-9

GOM GmbH (2020) GOM Correlate Professional

Groom LH, Leichti RJ (1994) Effect of adhesive stiffness and thickness on stress distributions in structural finger joints. J Adhes 44:69–83. https://doi.org/10.1080/00218469408026617

Habipi B, Ajdinaj D (2015) Wood finger-joint strength as function of finger length and slope positioning of tips. Int J Eng Appl Sci 2:

Harte A (2016) Chapter 60: Timber engineering: an introduction. In: ICE manual of Construction Materials. pp 707–715

Hernández R, Coman R, Beauregard RL (2011) Influence of machining parameters on the tensile strength of finger-jointed high-density black spruce lumber. Wood Fiber Sci J Soc Wood Sci Technol 43:2–10

Hu N, Li X, Wu Y, Zhou X (2012) Effects of finger length on finger joint process of glued laminated timber. In: Proceedings of 2012 International Conference on Biobase Material Science and Engineering. IEEE, pp 288–291

ISO 2555:2018. Plastics-Resins in the Liquid State or As Emulsions or Dispersions—Determination of Apparent Viscosity by the Brookfield Test Method. International Organization for Standardization ISO, Geneva

Jokerst RW (1981) Finger-Jointed Wood Products. United States Department of Agriculture. Forest Products Laboratory, 382. Madison Wisconsin (USA)

Khelifa M, Celzard A, Oudjene M, Ruelle J (2016) Experimental and numerical analysis of CFRP-strengthened finger-jointed timber beams. Int J Adhes Adhes 68:283–297. https://doi.org/10.1016/j.ijadhadh.2016.04.007

Khennane A, Khelifa M, Bleron L, Viguier J (2014) Numerical modelling of ductile damage evolution in tensile and bending tests of timber structures. Mech Mater 68:228–236. https://doi.org/10.1016/j.mechmat.2013.09.004

Lava P, Cooreman S, Coppieters S et al (2009) Assessment of measuring errors in DIC using deformation fields generated by plastic FEA. Opt Lasers Eng 47:747–753. https://doi.org/10.1016/j.optlaseng.2009.03.007

Milch J, Brabec M, Sebera V, Tippner J (2017) Verification of the elastic material characteristics of Norway spruce and European beech in the field of shear behaviour by means of Digital Image Correlation (DIC) for finite element analysis (FEA). Holzforschung 71:405–414. https://doi.org/10.1515/hf-2016-0170

Morin-Bernard A, Blanchet P, Dagenais C, Achim A (2021) Glued-laminated timber from northern hardwoods: Effect of finger-joint profile on lamellae tensile strength. Constr Build Mater 271:121591. https://doi.org/10.1016/j.conbuildmat.2020.121591

Ostapska K, Malo KA (2021a) Calibration of a combined XFEM and mode I cohesive zone model based on DIC measurements of cracks in structural scale wood composites. Compos Sci Technol 201:108503. https://doi.org/10.1016/j.compscitech.2020.108503

Ostapska K, Malo KA (2021b) Crack path tracking using DIC and XFEM modelling of mixed-mode fracture in wood. Theor Appl Fract Mech 112:102896. https://doi.org/10.1016/j.tafmec.2021.102896

Oudjene M, Khelifa M (2009) Finite element modelling of wooden structures at large deformations and brittle failure prediction. Mater Des 30:4081–4087. https://doi.org/10.1016/j.matdes.2009.05.024

Özçifçi A, Yapıcı F (2008) Structural performance of the finger-jointed strength of some wood species with different joint configurations. Constr Build Mater 22:1543–1550. https://doi.org/10.1016/j.conbuildmat.2007.03.020

Python Core Team (2015) Python: A dynamic, open source programming language

Quanjin M, Rejab MRM, Halim Q et al (2020) Experimental investigation of the tensile test using Digital Image Correlation (DIC) method. Mater Today Proc 27:757–763. https://doi.org/10.1016/j.matpr.2019.12.072

Serrano E, Gustafsson PJ (1999) Influence of bondline brittleness and defects on the strength of timber finger-joints. Int J Adhes Adhes 19:9–17. https://doi.org/10.1016/S0143-7496(98)00048-7

Rao S, Gong M, Cui YH, Mohammad M (2012) Effect of geometric parameters of finger joint profile on ultimate tensile strength of single finger-joined boards. Wood Fiber Sci J Soc Wood Sci Technol 44:263–270

Strickler MD (1980) Finger-jointed dimension lumber: past, present, and future. For Prod J 30:51–56

Tran VD, Oudjene M, Méausoone PJ (2014) FE analysis and geometrical optimization of timber beech finger-joint under bending test. Int J Adhes Adhes 52:40–47. https://doi.org/10.1016/j.ijadhadh.2014.03.007

Wood Handbook (2010) Wood handbook : Wood as an engineering material. Centennial edition. Madison, WI : U.S. Dept. of Agriculture, Forest Service, Forest Products Laboratory, (2010) ©2010, Madison Wisconsin (USA)

Yeh MC, Lin YL (2012) Finger joint performance of structural laminated bamboo member. J Wood Sci 58:120–127. https://doi.org/10.1007/s10086-011-1233-7